Available online at www.sciencedirect.com
SciVerse ScienceDirect
www.elsevier.com/locate/jmbbm

Research Paper

Development of novel aligned nanofibrous composite membranes for guided bone regeneration

M. Kharaziha[a,b,*], M.H. Fathi[a,c], H. Edris[a]

[a]Biomaterials Research Group, Department of Materials Engineering, Isfahan University of Technology, Isfahan 8415683111, Iran
[b]Department of Materials Engineering, Isfahan University of Technology, Isfahan 8415683111, Iran
[c]Dental Materials Research Center, Isfahan University of Medical Sciences, Isfahan, Iran

ARTICLE INFO

Article history:
Received 17 January 2013
Received in revised form
24 March 2013
Accepted 28 March 2013
Available online 17 April 2013

Keywords:
Nanofibrous membrane
Guided bone regeneration
Electrospinning
Forsterite nanopowder

ABSTRACT

The ability to mimic the structure of the natural extracellular matrix is a successful key for guided bone regeneration (GBR). For the regeneration of highly organized structures such as heart and bone, aligned fibrous membranes could provide anisotropic mechanical and biological properties which are adequate topographic guidance to cells. Here, novel nanofibrous membranes were developed through electrospinning of PCL-forsterite nanopowder. The membranes were characterized with regard to structural and mechanical properties, degradation, bioactivity and cellular interactive responses. Results showed that optimized nanofibrous composite membrane with significantly improved tensile strength and elastic modules was achieved through addition of 10 wt% forsterite nanopowder into PCL membrane. Addition of forsterite nanopowder decreased the average fiber diameters from 872±361 nm (pure PCL membrane) to 258±159 nm (PCL-10 wt% forsterite membrane). At higher forsterite contents (>10 wt%), the agglomeration of nanoparticles was observed which resulted in reduced mechanical properties. Aligned fibrous membranes revealed smaller fiber sizes and significantly enhanced and anisotropic mechanical properties compared to random ones suggesting that fiber alignment has a profound effect on the structural properties of membranes. Forsterite nanopowder increased the degradation rate showing enhanced hydrophilicity and induced apatite formation in simulated body fluid. Furthermore, composite nanofibrous membranes possessed significantly improved cellular responses in terms of attachment, proliferation and mineralization of pre-osteoblasts compared to PCL membrane. Thus, the currently developed nanofibrous composite membranes embedded in forsterite nanopowder expected to be attractive in GBR membrane applications.

1. Introduction

Guided bone regeneration (GBR) has been proposed as an effective therapy to repair the alveolar and mandible bone defects. In this therapy, a membrane is applied to encourage new bone ingrowth in the defected site while preventing the formation of fibrous tissue (Park and Wang, 2007). GBR membranes require enough flexibility to adapt to the bone

*Corresponding author at: Isfahan University of Technology Biomaterials Research Group, Department of Materials Engineering Isfahan 8415683111 Iran. Tel.: +98 3912750; fax: +98 3912752.
E-mail address: Kharaziha.ma@yahoo.com (M. Kharaziha).

1751-6161/$ - see front matter © 2013 Elsevier Ltd. All rights reserved.
http://dx.doi.org/10.1016/j.jmbbm.2013.03.025

defect shape and stiffness to maintain the space for bone regeneration (Obata et al., 2010). Fibrous membranes with inherent flexibility and highly interconnected porosity allowing efficient transport of nutrient materials and oxygen into and metabolic waste out of the regeneration site could be a good candidate as GBR membranes (Poologasundarampillai et al., 2011). Electrospinning has been emerged as a useful technique for developing fibrous structures due to ease of use, ability to fabricate random and aligned structures and control fiber diameters ranging from nano to micrometer. Furthermore, studies have demonstrated that nanofibrous structures could promote cellular attachment and proliferation (Liang et al., 2007).

A successful bone regeneration approach depends on the applied biomaterials to serve as a temporary matrix for cell proliferation, differentiation and mineralization of the extracellular matrix (ECM). For GBR application, fabrication of pure synthetic or natural polymer scaffolds is limited. It is mainly due to low stiffness, hydrophobic nature, relatively low bioactivity and degradation products of synthetic polymers which are detrimental for newly grown tissue, and high degradation rate of natural polymers (Jose et al., 2009). Furthermore, according to the natural bone structure consisting of hydroxyapatite (HA) embedded in a collagen matrix, a combination of a synthetic or natural polymer and a bioactive ceramic could provide enhanced mechanical properties and hydrophilicity, induced osteoconductivity and/or osteoinductivity, and improved cellular affinities (Fujihara et al., 2005; Webster et al., 2000).

So far, various polymeric fibrous compositions have been utilized as GBR membranes with the intention of achieving better mechanical properties and cellular attachment, proliferation, and mineral formation. Compared to inorganic bioactive ceramics, HA has been widely investigated as filler for electrospun synthetic and natural polymeric matrices such as poly (lactic acid) (Deng et al., 2007), poly(ε-caprolactone) (Thomas et al., 2006), collagen (Du et al., 1999; Thomas et al., 2007) and gelatin (Kim et al., 2005). Du et al., 1999 fabricated collagen-HA composite structures similar to the nanostructure of natural bone. However, they revealed mechanically weaker properties than bone structure. Furthermore, collagen easily degraded and adsorbed by the biological fluid. Compared to natural polymers, synthetic polymers exhibited higher mechanical properties with controllable degradation rate. For instance, PCL has been widely applied to develop scaffolds for GBR membranes due to high mechanical strength, flexibility, degradation with compatible rate with bone regeneration and biocompatibility (Woodruff and Hutmacher, 2010). Wide range of studies has been focused on the development and characterization of nanofibrous HA-PCL scaffolds using an electrospinning technique (Bishop et al., 2006; Fu et al., 2012; Thomas et al., 2006; Tyagi et al., 2009; Lehmann et al., 2010; Yang et al., 2009). On the other hand, other inorganic bioactive materials such as calcium carbonate and TCP (Fujihara et al., 2005; Catledge et al., 2007) were also utilized for GBR membranes. Fujihara et al. found that PCL-calcium carbonate fibrous scaffolds revealed better alkaline phosphatase expression and osteocalcin than PCL-HA (Fujihara et al., 2005). However, low mechanical properties for bone tissue repair, random orientation of fibers and poor dispersion of HA particles are still the most important limitations related to the present polymer/bioactive ceramic fibrous membranes.

Forsterite with chemical formula Mg_2SiO_4 has been introduced as dental ceramics due to high compression strength and high Young's modulus (Denry, 1996; Ni et al., 2007). Our recent studies show the nano-sized forsterite is a bioactive ceramic, which could promote cell proliferation compared to tissue culture plate (TCP) (Kharaziha and Fathi, 2009; Kharaziha and Fathi, 2010). Furthermore, it shows superior mechanical properties than micron-sized forsterite and other bioactive ceramics such as HA (Kharaziha and Fathi, 2010). As nano-sized ceramics mimic the dimension of mineral crystals in the natural tissue and demonstrated to induce higher protein absorption and cell adhesion compared to their micro-sized counterparts due to higher surface area (Yang et al., 2009; Webster et al., 2000), it is expected that the membranes consisting of nano-sized forsterite can be good a candidate for GBR application. Recently, we have fabricated PCL-forsterite nanocomposites scaffolds through solvent-casting/particle-leaching technique (Diba et al., 2011; Diba et al., 2012). However, mimicking the highly oriented ECM structure in terms of architecture is the vital factor for guided bone regeneration applications. Therefore, it is envisioned that biocomposite nanofibrous membranes containing forsterite developed by electrospinning might be suitable as GBR membranes as they could mimic the architectural of bone ECM and improve the mechanical properties compared to previous fibrous membranes. In addition to advantages of fibrous membranes, results demonstrated that aligned fibrous membranes guided the cells to grow at specific orientation (Xu et al., 2004). For this aim, in this paper novel nanofibrous PCL-forsterite membranes were developed in the two architectures (aligned and random fibrous membranes) and their mechanical and structural properties and in vitro bioactivity and degradation of membranes were evaluated. Subsequently, pre-osteoblast cells were cultured on the aligned fibrous membranes, and the effects of chemical and mechanical properties of membranes on the cellular attachment, proliferation and mineralization were also investigated.

2. Materials and methods

2.1. *Fabrication of nanofibrous PCL-forsterite membranes*

PCL-forsterite composite fibrous membranes with variable compositions were prepared by using electrospinning setup. Forsterite nanopowder was synthesized through the sol–gel process described in our previous report (Kharaziha and Fathi, 2009) and presented at Fig. 1 (a). Briefly, water-based solutions of the magnesium salts and colloidal silica were prepared. Then, an aqueous solution of sucrose was added to the prepared solution. PVA solution was also added in to the final solution and the pH value was adjusted to 1. The solution was mixed homogeneously and heated at 80 °C for 2 h. The prepared gel was then heated at 100 °C in air for complete dehydration. Pure forsterite nanopowder was obtained through the calcination of the dried gel at 800 °C. TEM image (Fig. 1(b)) confirmed that forsterite nanopowder consisted of circle particles with an average diameter of 25–45 nm (Kharaziha and Fathi, 2009).

PCL solution was prepared at the concentration of 10%(w/v) in (9:1) chloroform: ethanol solution. After PCL dissolving, forsterite nanopowder was added at 5, 10 and 20 wt%

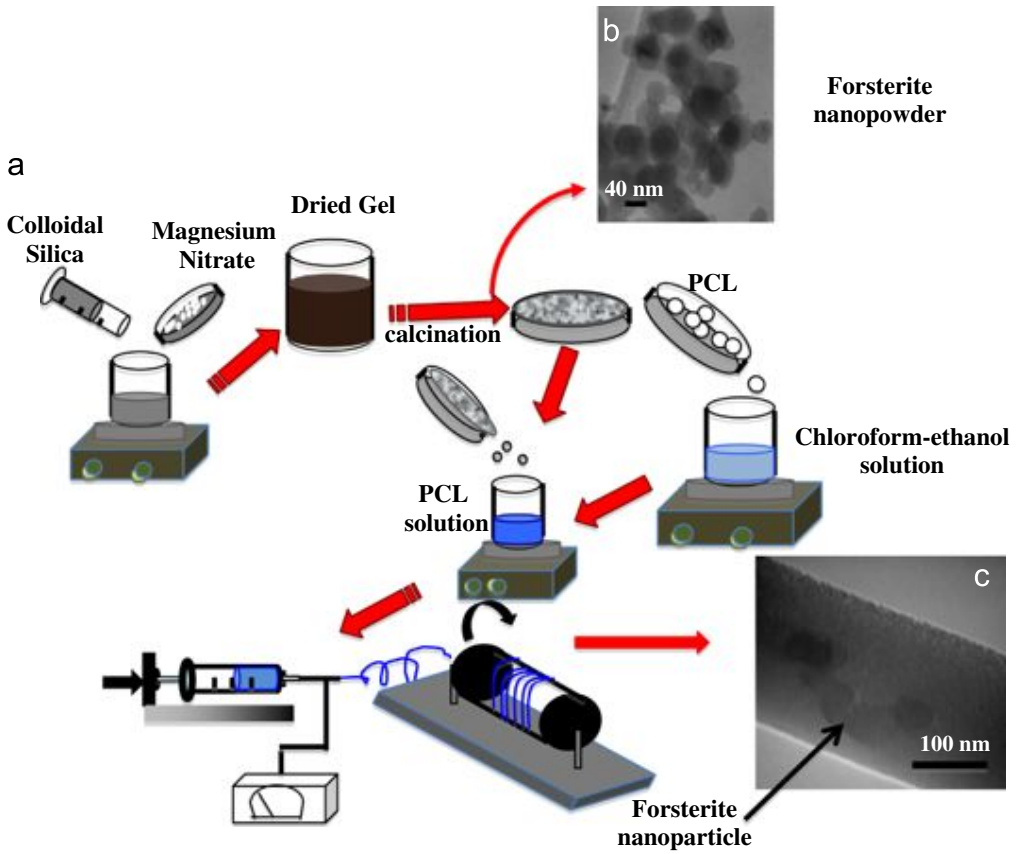

Fig. 1 – (a) Schematic of the strategy for fabrication and transmission electron micrograph of (b) forsterite nanopowder and (c) PCL-forsterite fibrous membrane.

concentrations in order to provide (P-5F), (P-10F) and (P-20F) solutions, respectively, and constant amount of 0.06% w/v NaCl was applied in order to increase conductivity of solutions. As prepared solutions were sonicated for 1 h and membranes were developed by electrospinning process as shown in Fig. 1(a). For the electrospinning process, the polymer solutions were fed at into a 1 mL standard syringe equipped with a 23 G blunted stainless steel needle using a syringe pump. The flow rate (2 mL/h), the distance between the needle and the collector (18 cm) and the electrospun voltage (20 kV) were optimized and kept constant during the electrospinning process. Aligned nanofibrous membranes (A) were spun and deposited on the rounded stainless steel drum (5 cm) rotating at a speed of 3750 rpm (corresponding linear velocity of 5 m s^{-1}) while the random fibers (R) were collected on the glass slide placed on the collector plate. The fabricated membranes were dried overnight under vacuum condition prior to further characterizations and biological experiments.

2.2. *Characterization of nanofibrous PCL-forsterite membranes*

The surface topographies of the fibrous membranes, were characterized by scanning electron microscopy (SEM) analysis using a Philips XL30 SEM. Samples were sputter-coated with a thin layer of gold and the SEM images along with NIH Image J software were used to determine the fiber and pore sizes ($n=50$) of the membranes. Furthermore, distribution of forsterite nanopowder in the fibers was evaluated by transmission electron microscopy (TEM). The chemical composition of the membranes was confirmed through Fourier-transform infrared spectroscopy (FTIR) (Bomem, MB 100) performed over a range of 600–4000 cm^{-1} and resolution of 2 cm^{-1} and X-ray diffraction (XRD) carried out using an X'Pert Pro X-ray diffractometer (Phillips, Netherlands) with CuKα radiation ($k=0.15406$ nm) at a generator voltage of 40 kV and a current of 40 mA. Additionally, thermogravimetric analysis (TGA) (Rheometric scientific 1998, USA) was carried out to confirm the real weight percent of forsterite nanopowder in the fibrous membranes.

The mechanical properties of membranes were determined by using uniaxial tensile testing technique (INSTRON, Zwick, United Kingdom) with 10 N load capacity at a rate of 7 mm/min. Samples were prepared in rectangular pieces with a length of 4–5 mm, width of 6–8 mm and thickness of 0.3–0.5 mm. At least 5 samples were prepared for each membrane composition. Tensile strength, tensile modulus, and strain at break were determined from the stress–strain curves. Tensile modulus was determined from the linear region of the stress–strain curve (5–10%), while strain at break was obtained when samples failed. Measured values were reported as mean standard deviation (SD).

2.3. *Degradation studies of the membranes*

In vitro degradation assay was used to study the weight loss of the membranes ($n=3$) with dimensions of 5 mm × 5

mm × 0.5 mm (length, width, thickness). The samples were incubated in Phosphate buffered saline (PBS) (Sigma) at 37 °C for 7, 14, 21 and 28 days. PBS was changed every 3 days. After each specific time point, the membranes were surface wiped and weighted (at wet state). Then, they were rinsed in PBS and lyophilized using a freeze-dryer for overnight. The weight of dried samples was also measured after lyphilization. The percent water absorption and weight loss for each sample were calculated according to Eqs. (1) and (2), respectively:

$$\text{Water Absorption} = 100 \times (w_a - w_0)/w_0 \quad (1)$$

$$\text{Weight Loss} = 100 \times (w_0 - w_t)/w_0 \quad (2)$$

Where W_0, W_a and W_t were the starting dry, wet and, dry (after removal) weights, respectively. Furthermore, pH values of the PBS solutions during immersing the membranes were also recorded by using Metrohm pH meter.

2.4. Bioactivity studies of the membranes

The bioactivity was assessed through the soaking of the membranes in simulated body fluid (SBF) prepared according to Kokubo protocol (Kokubo and Takadama, 2006). The samples ($n=3$) with dimensions of $5 \times 5\ cm^2$ and were put in the polyethylene containers and maintained at 37 °C upon a month. The formation of apatite layer on the membranes was verified by SEM coupled with Energy-Dispersive Spectroscopy (EDS). Furthermore, the bioactivity mechanism was evaluated by measuring the pH of solutions and Ca, Mg and P ions using inductively coupled plasma atomic emission spectroscopy (ICP) (AES; Varian, USA).

2.5. In-vitro cellular assays

In order to evaluating the in vitro osteoplastic responses in terms of the attachment, proliferation and mineralization on the fibrous membranes, MC 3T3-E1 pre-osteoblasts (sub-clone 14) were applied. The pre-osteoblast cells were cultured in Alpha Minimum Essential Medium (α–MEM, Cellgro, Mediatech, Manassas, VA, USA) supplemented with 10% fetal bovine serum (FBS, Cellgro, Mediatech, Manassas, VA, USA) and 1% streptomycin/ penicillin (Cellgro, Mediatech, Manassas, VA, USA). Before cell seeding, the fibrous membranes were sterilized under 30 min soaking in 70% ethanol, overnight UV light and finally immersed in culture medium overnight before cell seeding. Cells (within passages 18–20) at a density of $3 \times 10^4\ ml^{-1}$ were seeded onto the membranes. Culture medium was refreshed every 3 days and the culture medium was changed to osteogenic medium consisting of above culture medium supplemented with $50\ \mu g\ ml^{-1}$ ascorbic acid (Sigma-Aldrich) and 10 mM β-glycerophosphate (Fluka) after 2 weeks to induce differentiation from pre-osteoblast to osteoblast. Pre-osteoblast cells were also seeded on tissue culture polystyrene (TCP) as control.

The cell attachment on the membranes was determined using DNA quantification assay (Quant-iT™ PicoGreen®, Invitrogen, USA), according to the manufacturer's protocol. Membranes ($n=3$) were rinsed with Dulbecco's phosphate buffered saline (DPBS, Gibco, USA) and weighed at wet condition. The samples were then digested overnight at 60 °C in 1 mL of DNA extraction solution. In order to prepare DNA extracted solution, PBE buffer was prepared by dissolving Na_2HPO_4 and EDTA (Sigma-Aldrich) in deionized water and adjusting the pH to 6.5 using 1 M HCl solution. Following, L-cystein was added to 20 mL of DNA extracted solution and the prepared solution was mixed with papain (0.5%(v/v)). Finally, 1X PicoGreen solution (50% (v/v)) was added to digested sample solution (50% (v/v)) and their absorbance were measured at 485 nm wavelength.

The pre-osteoblast metabolic activity on the membranes was determined by using the Alamar blue (AB) assay according to the manufacturer's protocol (Invitrogen) at days 0 (6 h), 7, 14 and 21 of culture on fibrous scaffolds and tissue culture plate (TCP). Briefly, AB dissolved in warm culture medium was added into each well and incubated for 3 h. Then, reduced-color culture medium within each well was transferred to 96-well plate in duplicate and absorbance was measured at 544–590 nm wavelength. Finally, the normalized metabolic activity with respect to day 0 was calculated for each membrane. In order to confirm the Alamar blue data, PicoGreen assay was also evaluated according to above protocol.

Pre-osteoblast mineralization was assessed via alizarin red staining. Briefly, at various culture periods, cell–membrane constructs were rinsed with distilled water and fixed with 4% PFA for 20 min. After rinsing the samples, they were incubated with the alizarin red dye (Sigma-Aldrich) for 10 min at 4 °C for 24 h. After rinsing the samples to remove the excess alizarin red dye, samples were incubated with 10% CPC at room temperature for 30 min and the absorbance of the obtained solution, which is proportional to the amount of calcium de-posited, was read on a TECAN plate reader at 405 nm.

2.6. Statistical analysis

All the data were presented in mean ± standard deviation (SD) and statistical significance was measured by performing one-way ANOVA analysis followed by Tukey's multiple comparison using GraphPad, Prism Software (V.5). Differences were taken to be significant for *, \widehat, +: $P<0.05$.

3. Results and discussion

3.1. Fabrication and characterizations of the fibrous membranes

3.1.1. Morphology, fiber and pore sizes of fibrous membranes

PCL is a common polymer for bone tissue engineering because of the necessity of the structural stability. However, application of pure PCL as a backbone due to slow degradation and hydrophobicity is limited. Forsterite nanopowder was incorporated into PCL fibers by electrospinning process using chloroform/ethanol solution to form composite nanofibers. SEM images of random (Fig. 2(a)) and aligned (Fig. 2(b)) fibrous membranes clearly demonstrated that PCL fibrous membranes consisted of randomly oriented and aligned smooth fibers, respectively. The morphologies,
fiber size distributions (Fig. 2(c) and (d)) and average fiber diameters (Fig. 2(e) and (f)) of the membranes changed as a

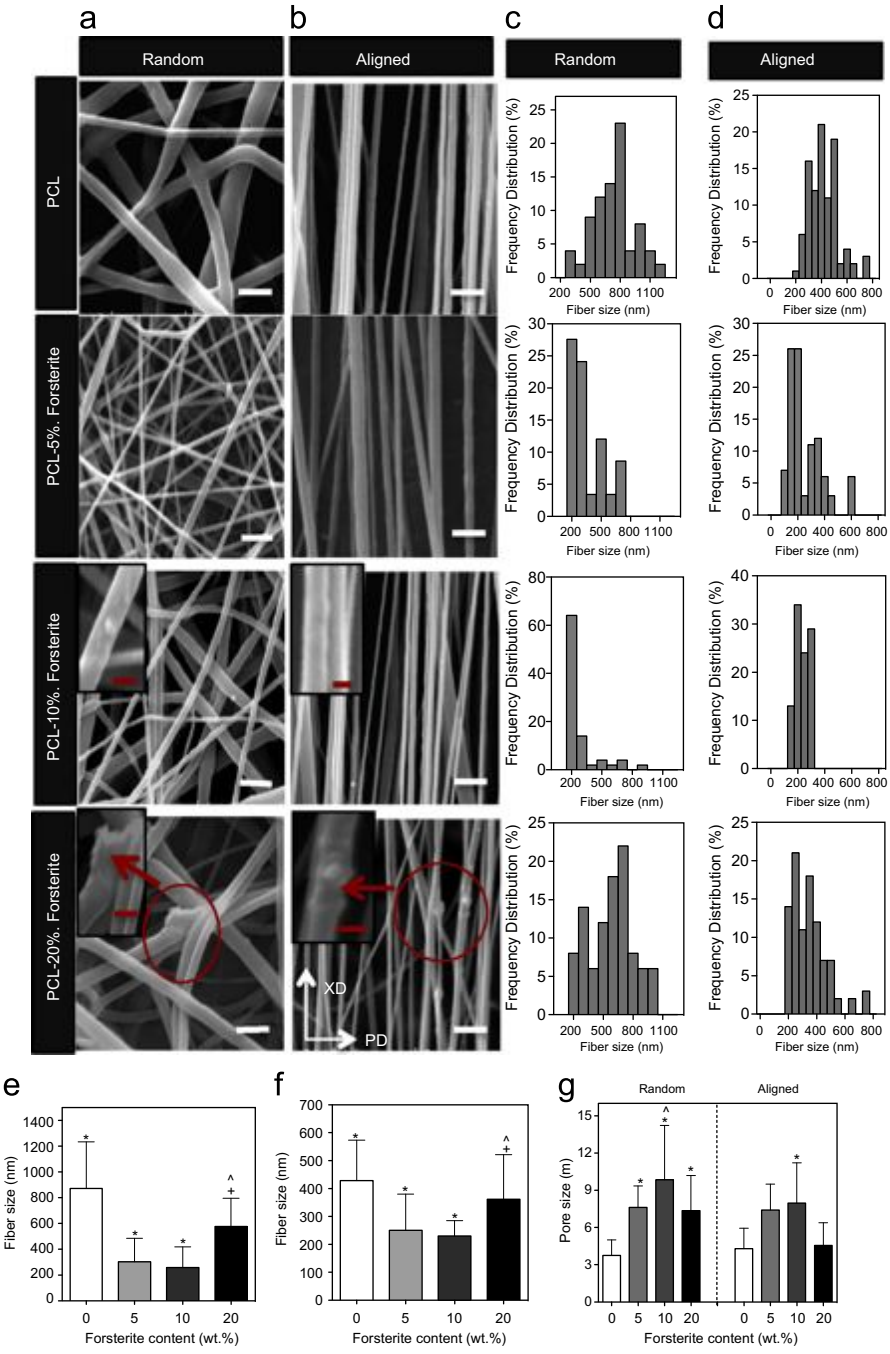

Fig. 2 – Structural properties of membranes: SEM micrographs of (a) random and (b) aligned fibrous membranes consisting various amount of forsterite nanopowder and (c,d) the corresponding fiber size distributions of the fibers shown in images (a) and (b), respectively (white scale bar = 2 μm and red scale bar = 500 nm). Average fiber size of (e) aligned and (f) random fibrous membranes. (g) Average pore sizes of fibrous membranes as function of forsterite content and the topography of membranes (Aligned and random) (*, ^: Significant difference compared to pure PCL and PCL-5 wt%forsterite membranes, respectively (*,^: $P < 0.05$)).

function of forsterite content and the topography of membranes (Aligned or random). Random fibrous membranes revealed larger fiber diameters with more extended fiber size distribution than aligned ones due to the stretching effects of the high speed rational during the collection of fibers on the drum. Overall, the surfaces of fibers were turned rougher by increasing forsterite content and the inclusion of forsterite nanopowder upon 10 wt% reduced significantly ($P < 0.05$) the average fiber diameter and distribution. While the average fiber diameters of R(PCL) and A(PCL) were about 872 ± 361 nm and 382 ± 97 nm, respectively, they were dramatically decreased to about 258 ± 159 nm and 232 ± 51 nm within R(P-10F) and A(P-10F) membranes, respectively (TEM micrograph of A(P-10F) also confirmed the average fiber sizes at 220–250 nm with fairly homogenous dispersion of forsterite nanopowder (Fig. 1(c))). Similar result was also reported for

Poly-L-lactic acid/hydroxyapatite fibrous membrane (Sui et al., 2007). Under the same electrospinning parameters, fiber diameters were determined by the characteristic parameters of the initial electrospinning suspensions such as conductivity. Presence of forsterite nanopowder upon 10 wt% might be provide enhanced charge density of the suspension resulted in fabrication of more uniform and smaller fibers. However, more forsterite content (upon 20 wt%) (R(P-20F) and A(P-20F) membranes) resulted in enhanced average fiber diameters and distributions due to the agglomeration of nanoparticles ranging from 200 to 600 nm as recognized using circles at Fig. 2(a) and (b). As such agglomerates were not observed in the composite nanofibrous membranes loaded with less forsterite content.

The pore sizes of membranes were also influenced by the presence of forsterite nanopowder (Fig. 2(g)). At both aligned and random fibrous membranes, with increasing forsterite content upon 10 wt% forsterite, the average pore size significantly ($P<0.05$) enhanced and then reduced at (P-20f) membranes. Specifically, the pore sizes of random fibrous membranes increased from 4.4 ± 1.2 μm within R(PCL) to 10.1 ± 3.2 μm on R(P-10F) membrane. Furthermore, no significant difference was observed between the average pore sizes of aligned and random fibrous membranes with the same compositions. Increased average pore size might be due to decreased fiber sizes of membranes with increasing forsterite content upon 10 wt%. Additionally, reduced pore sizes at high forsterite loading might also be due to the agglomeration of forsterite nanopowder.

3.1.2. *Chemical characterization of fibrous membranes*

Chemical characterization and functional groups of pure PCL and nanofibrous composite membranes were conducted using FTIR analysis (Fig. 3(a)). Pure PCL spectrum revealed the peaks corresponding to PCL including two main bands at 1726 cm^{-1} (stretching vibrations of the carboxyl (C═O)) and 1180 cm^{-1} (stretching vibrations of the ether groups (C–O–C)) with other bands such as C–O stretching vibrations at 1050 cm^{-1}, asymmetric C–O–C stretching at 1244 cm^{-1}, symmetric C–H stretching at 2865 cm^{-1} and C–O and C–C stretching at 1296 cm^{-1}. In the spectra of composite membranes, in addition to PCL bands, the characteristic absorption band of forsterite were observed at 870 cm^{-1} corresponded to Si–O–Si bond. With increasing forsterite content, other characteristic bands at 830–1000 cm^{-1} appeared which belonged to the various vibration modes of Si–O–Si bonds (Diba et al., 2011). Compared to FTIR spectrum of pure PCL, the spectra of composite membranes indicated a number of PCL bands shifted to higher wavenumbers which might be due to formation of hydrogen bonds between the specific groups of forsterite and PCL.

X- ray diffraction patterns of nanofibrous composite membranes (Fig. 3(b)) demonstrated the presence of the characteristic peaks of forsterite at $2\theta=20.9°$, 23.77°, 27.72° and 35.32°. The crystal structure of PCL revealed two intensive and sharp peaks at $2\theta=21.03°$ and 23.7° which their intensity gradually weakened and shifted by increasing

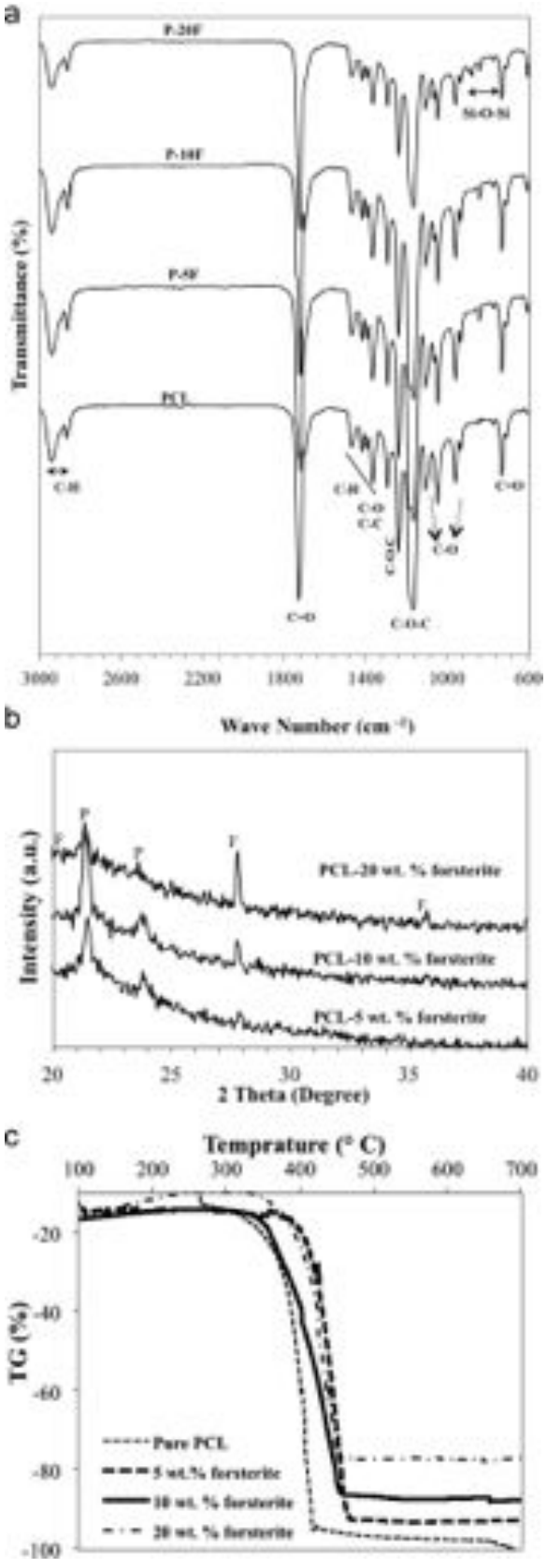

Fig. 3 – Chemical properties of fibrous membranes as a function of forsterite content: (a) FTIR spectra, (b) XRD patterns spectra and (c) TGA curve of fibrous membranes.

forsterite content. This result showed the interaction between PCL and forsterite nanopowder.

The true content of forsterite nanopowder in the membranes was determined by TGA and the remained weight percentage of membranes after completely burning out of PCL content (Fig. 3(c)). Results showed that thermal decomposition of PCL started at 320 °C and continued up to 460 °C accompanied by significant weight losses recorded for (PCL), (P-5F), (P-10F) and (P-20F) which were about 97.92%, 93.13%, 87.25% and 77.54%, respectively. They confirmed that the amount of forsterite nanopowder added to the starting solution prior to electrospinning was approximately similar to its percentage in the membranes after electrospinning.

3.1.3. *Mechanical characterization of fibrous membranes*

The mechanical properties of membranes were strongly affected by the membrane architecture and forsterite content. The typical stress–strain curves of random fibrous PCL and composite membranes (Fig. 4(a)) exhibited similar trends; obeyed Hooke's law in the beginning of the curves (strain $<7\%$) continued with elastic to plastic transitional patterns. As strain continuously increased, the curves deviated from the linear proportionality and, depending on the forsterite content, they showed various amounts of ultimate strength and strain at break. On the other hand, the stress–strain curves of aligned fibrous membranes at preferred (PD) and orthogonal cross-preferred (XD) directions confirmed the anisotropic mechanical properties (Fig. 4(b) and (c)) as their tensile modulus in PD direction were significantly higher ($P<0.05$) than those of the corresponding samples along XD direction which could be useful for guided bone regeneration.

Tensile modulus, ultimate strength and strain at break of aligned and random fibrous membranes calculated from the curves and presented at Fig. 4((c)–(f)) suggested that they reached peak values when forsterite nanopowder content exceeded 10 wt%. Tensile modulus (Fig. 4(d)) of PCL membranes increased from 5.33 ± 0.9 MPa on R(PCL) to 11.12 ± 3.3 MPa on R(P-10F) and from 6.98 ± 1.1 MPa on A(PCL) to 20.8 ± 7.3 MPa within A(P-10F) membrane due to an additional energy-dissipating mechanism introduced by the nanoparticles in PCL matrix and reported in other composite membranes(Lee et al., 2010; Yang et al., 2009). Additionally, strain at break increased significantly from $33.93\pm7.5\%$ within R(PCL) to $64.13\pm7.9\%$ on R(P-10F) and from $66.25\pm7.4\%$ within A(PCL) to $98.46\pm9.4\%$ within A(P-10F) ($P<0.05$). This plasticization behavior at low forsterite content was also reported for other nanofibrous composite membranes containing HA as filler (Yang et al., 2007; Bianco, et al., 2009). For instance, Bianco et al. reported this behavior at low HA content in PCL matrix. However, they did not show improvement of tensile modulus and tensile strength (Bianco et al., 2009). Li et al. also demonstrated that silica significantly improved tensile modules and tensile strength while strain at break decreased compared to pure PCL fibrous membrane (Lee et al., 2010). Compared to both of the above membranes, PCL-forsterite revealed better tensile modulus and strain at break demonstrating the potential of this membrane for GBR application.

When forsterite nanopowder content reached 20 wt%, tensile modulus of fibrous membranes decreased to 3.14 ± 0.9 MPa on R(P-20F) and 17.45 ± 2.6 MPa on A(P-20F) and strain at break decreased to $38.49\pm1.7\%$ on R(P-20F) and 54.68 ± 9.3 on A(P-20F), respectively, due to the presence of nanoparticle agglomeration and heterogeneity of the structures (as observed at Fig. 2(a) and (b)). Previous results on PCL-based electrospun membranes also reported that the reduced strain at break within higher amount of filler due to a quasi- brittle behavior (Fujihara at al. 2005; Low et al., 2008).

3.2. *In-vitro bioactivity of the fibrous membranes*

Besides mechanical properties, osteo-conductivity is another important characteristic of membranes for bone tissue engineering application. This property was evaluated by studying the apatite formation ability on the surface membranes by incubation in SBF with ion concentrations equal to human blood plasma. SEM micrographs of PCL and composite membranes after 30 days incubation in the SBF confirmed while PCL could not induce bone-like apatite formation (Fig. 5(a)), spherical particles covered the surfaces of nanofibrous composite membranes (Fig. 5(b)–(e)) which contained Ca and P ions according to EDS analyses (Fig. 5(f)). The Ca/P ratio was 1.59, 1.51 and 1.43 for A(P-5F), A(P-10F) and A(P-20F), respectively, which closed to this ratio at HA structure ($Ca/P=1.63$). Additionally, bone-like apatite formation process on A(P-20F) and A(P-10) membranes (Fig. 5(c) and (d)) was much faster than that of on the A(P-5F) membrane (Fig. 5(b)) as the membranes were partially covered by spherical particles.

In order to explain the bioactivity mechanism on the fibrous membranes, the cumulative variation of ion concentrations consisting of magnesium released from composites into SBF, calcium and phosphorus ions deposited from SBF on the surface membranes were estimated. According to Fig. 5 (g), dissolved magnesium ions increased while more calcium and phosphorus ions decreased with increasing forsterite content. Furthermore, increased pH value at the beginning of incubation time confirmed magnesium ions dissolution (Fig. 5(h)). The released magnesium ions acted as nucleation sites for the deposition of calcium and phosphorus ions and formation of bone-like apatite on the surface of fibrous membranes. This process also accompanied by decreasing pH value of SBF solution exposed to composite fibrous membranes (Fig. 5(h)). According to our recent results, forsterite nanopowder was bioactive ceramic (Kharaziha and Fathi, 2009) and introducing it could be proved to stimulate osteo-conductivity through dissolution Mg ions and the formation of nuclei site for Ca and phosphorus ions deposition on the composite fibrous membranes.

3.3. *In-vitro degradation of the fibrous membranes*

Slow degradation rate of PCL is one of the most important issues in application of this polymer for bone tissue engineering field. According to Fig. 6, the degradation rate of the membranes could be modulated by addition of forsterite nanopowder and could be optimized according to the application through various forsterite loading. The weight losses of the membranes significantly ($P<0.05$) increased with both incubation time and forsterite content upon 10 wt% (Fig. 6 (a)). At the end of the incubation, the weight losses of membranes were around $5.31\pm0.8\%$, $12.68\pm1.2\%$,

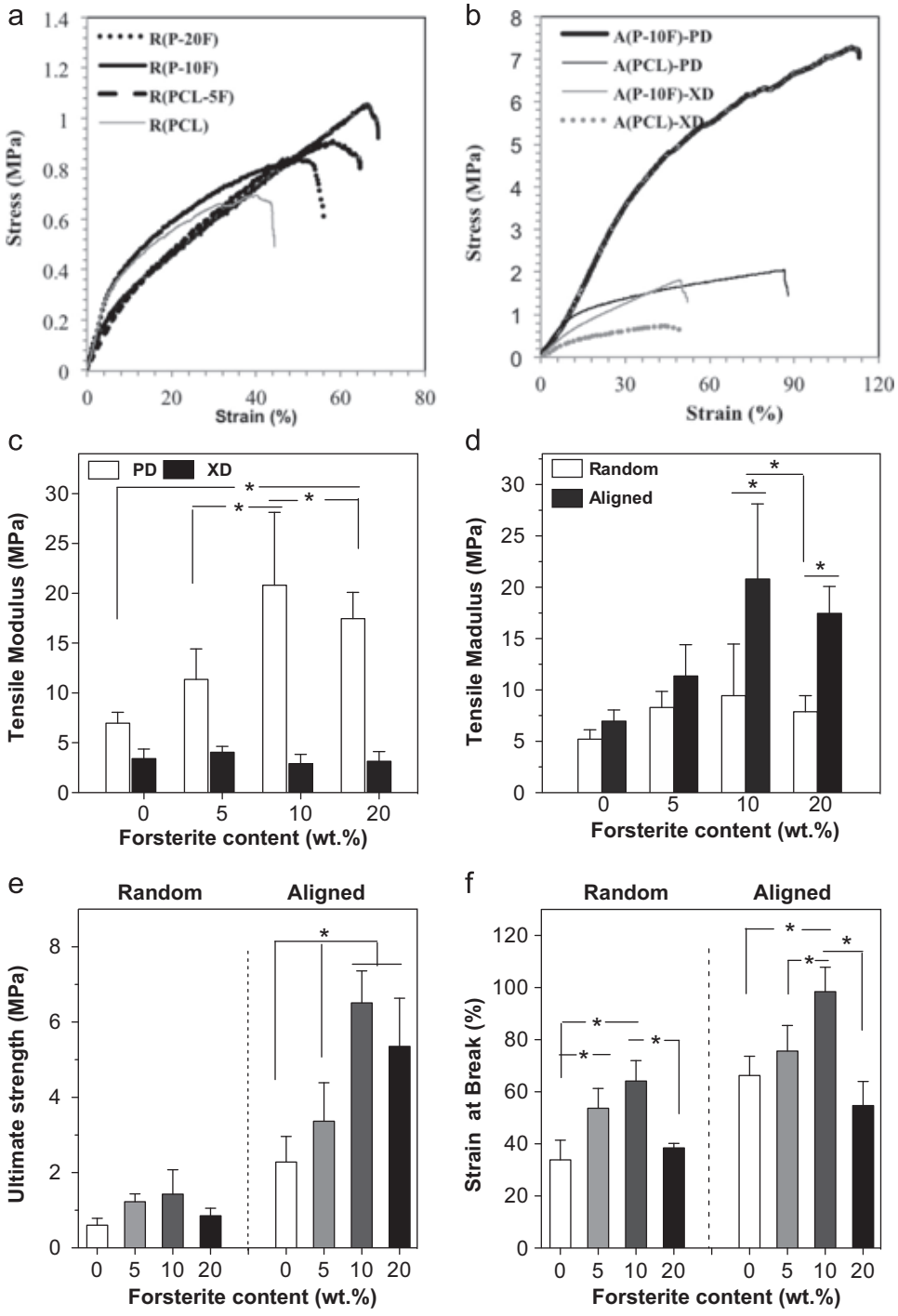

Fig. 4 – Effects of topographical (aligned and random) and chemical (forsterite content) cues on the mechanical properties: representative stress–strain curves of (a) random membranes consisting of 0, 5, 10 and 20 wt% forsterite and (b) aligned PCL and PCL-10 wt%forsterite (P-10F) membranes at preferred (PD) and orthogonal cross-preferred (XD directions). (c) Tensile modulus of aligned membranes at PD and XD directions. (d) Tensile modulus, (e) ultimate strength and (f) strain at break of aligned and random fibrous membranes as functions of forsterite content and the topography of membranes (Aligned and random) (*: significant difference between groups (*: $P<0.05$)).

27.88±3.2% and 21.55±5.6% within the A(PCL), A(P-5F), A(P-10F) and A(P-20F) membranes, respectively. As expected, due to the hydrophobicity of PCL, the weight loss of (PCL) membrane was quite slow and higher weight loss of A(P-10F) than (PCL) originated from leaching out of forsterite nanoparticles which accompanied by increasing the porosity of the membranes and hydrolytic attacks of their surfaces. Additionally, A(P-20F) membrane showed less weight

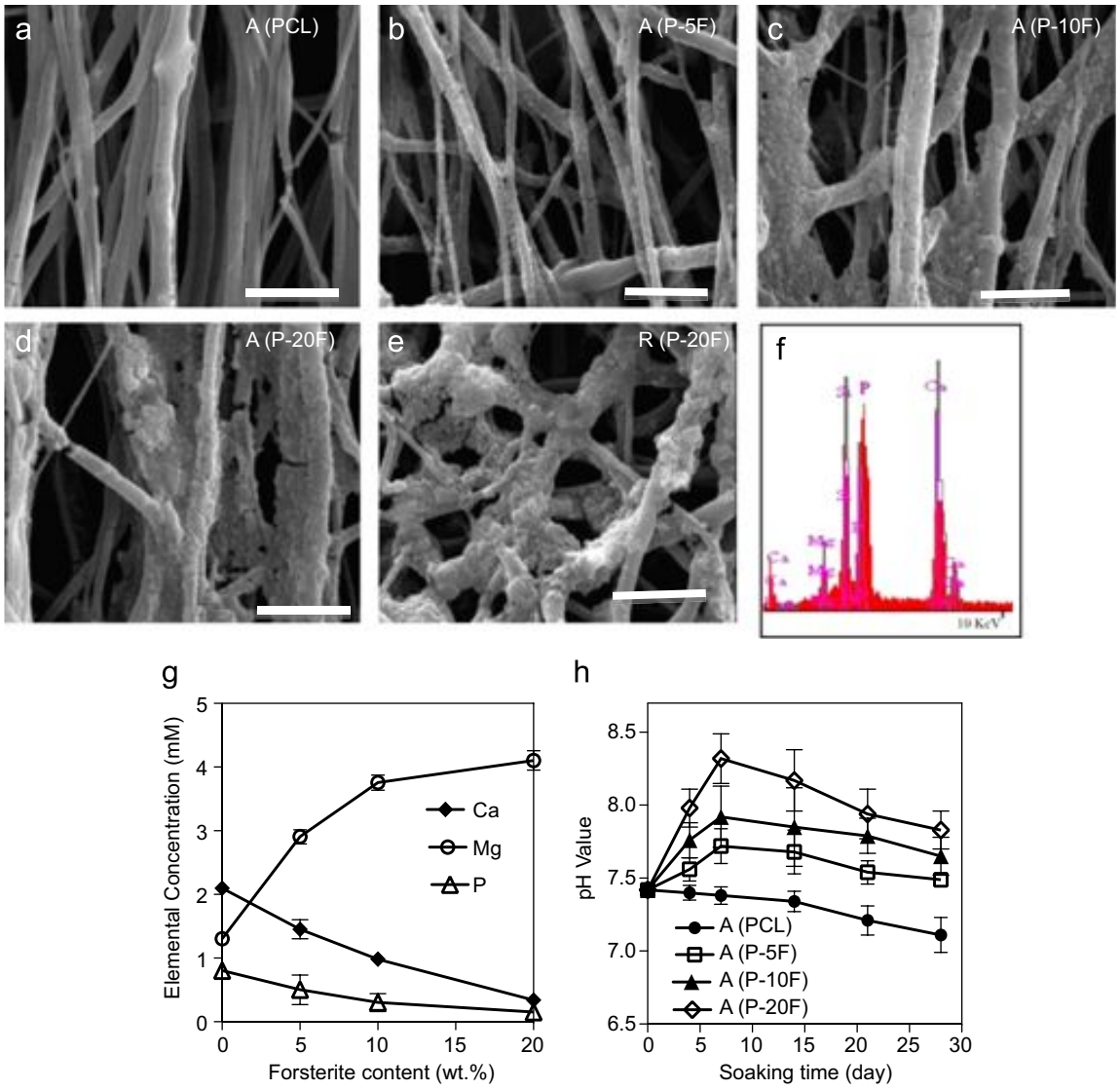

Fig. 5 – Effects of forsterite content on the bioactivity of membranes: SEM micrographs of (a) aligned PCL (A(PCL)), (b) aligned PCL-5 wt%forsterite (A(P-5F)), (c) aligned PCL-10 wt%forsterite (A(P-10F)), (d) aligned PCL-20 wt%forsterite (A(P-20F)) and (e) random PCL-20 wt%forsterite (R(P-20F)) membranes showing apatite formation on the fibrous membranes after 4-week SBF immersion (scale bar = 5 μm). (f) Representative EDS spectrum of A(P-20F) fibrous membrane. (g) Ca, Mg and P ion concentrations of SBF solution after 4 weeks immersion of the various membranes and (h) pH value trends of SBF solution during immersion of the various membranes.

loss than that of A(P-10F) which might be due to reduced pore sizes of membrane as shown in Fig. 2(g).The degradation behavior was also confirmed by water absorption results (Fig. 6(b)). It was observed that the water absorptions of the nanofibrous composite membranes consisting of more than 10 wt% forsterite were significantly ($P<0.05$) higher than that of A(PCL) and A(P-5F) membranes at all time periods. The water absorption of (PCL) membrane gradually increased upon 47.42±10.5% after 21 days of incubation. After that, it decreased and finally reached to 37.7±10% while at other composite fibrous membranes (for examples A(P-10F)), the highest water absorption values were obtained at day 7 of incubation (125.1±15%) and then decreased to 71.6±5%.

When (PCL) membrane was immersed in PBS, pH value of PBS also revealed a decreased trend from an initial value (7.4) to 7.2 after a month of incubation due to the release of acidic groups from (PCL) membrane degradation (Fig. 6(c)). While this trend was different for the nanofibrous composite membranes. The pH values increased from 7.4 to 7.48, 7.58 and 7.65 within A(P-5F), A(P-10F) and A(P-20F) membranes, respectively, after five days incubation due to the release of alkaline ions. Then, it slightly decreased to 7.32, 7.38 and 7.41 for A(P-5F), A(P-10F) and A(P-20F) membranes, respectively, at the end of incubation period correlated to locally naturalization of the acidification of the medium due to acidic products of PCL degradation by the dissolution of Mg ions. This suggested that forsterite nanopowder could locally

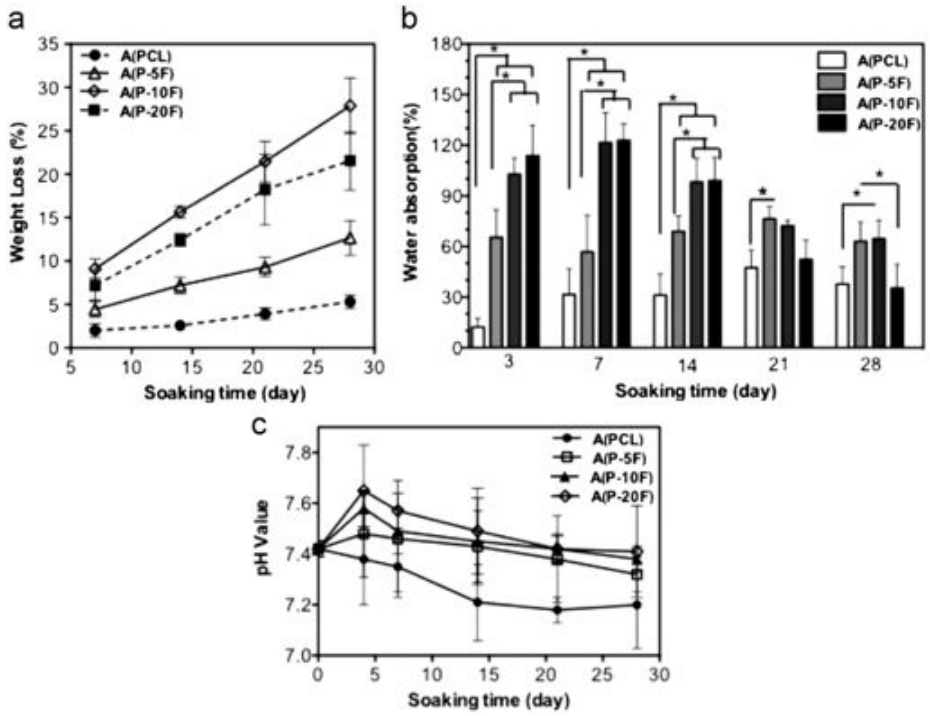

Fig. 6 – Effects of forsterite content on the in vitro degradation of fibrous membranes: (a) weight loss and (b) water absorption of aligned fibrous membranes as function of soaking time and (c) pH trends of PBS during the immersing of the membranes (*: Significant difference between groups (*: $P<0.05$)).

compensate the acidic degradation products of PCL matrix and turned the medium to alkalinity due to their dissolution by-products.

3.4. *In-vitro cellular interactive responses to the fibrous membranes*

As the topography of fibers plays an important role in regulating the cell behavior, in order to mimic the structure of bone ECM, cellular behavior was investigated on the aligned fibrous membranes. To assess the behavior of cells on composite membranes, we primarily analyzed attachment of MC-3T3 cells that were cultured for 6 h on the developed membranes. DNA quantification (PicoGreen assay) data confirmed that higher forsterite nanopowder loading (upon 10 wt%) significantly enhanced cell attachment compared to PCL membrane ($P<0.05$) (Fig. 7(a)). For instance, compared to pure (PCL), cell attachment increased 4-folds at A(P-20F) membrane. The proliferation of MC-3T3 cells was also evaluated after 7, 14 and 21 days of culture on different membranes by DNA assay (Fig. 7(a)). Overall, DNA content enhanced with increasing culture time. At all culture time, DNA content, which is proportional to cell number, significantly ($P<0.05$) enhanced on A(P-10F) and A(P-20F) membranes compared to pure (PCL). The cell proliferation on the composite fibrous membranes was found to be 105%, 120% and 127% within A(P-5F), A(P-10F) and A(P-20F) membranes, respectively, compared to (PCL) membrane after 21 days of culture. Furthermore, cell proliferation on A(P-20F) was significantly ($P<0.05$) greater than A(P-5F) membrane.

The normalized metabolic activity of MC-3T3 cells cultured on the membranes also confirmed PicoGreen assay (Fig. 7(b)). In general, the metabolic activity of MC-3T3 cells grown on the all membranes increased by the culture time. However, before 14-day culture, there was no significant difference between all groups. At day 21 of culture, the normalized metabolic activity of MC-3T3 cells on the composite fibrous membranes was significantly more than PCL fibrous membrane. Furthermore, compared to cells cultured on TCP applied as control, MC-3T3 cells cultured on A(P-10F) and A(P-20F) membranes revealed significantly ($P<0.05$) higher metabolic activity. Our data confirmed that forsterite nanopowder incorporated nanofibrous membranes had remarkably favored cell growth and provided a suitable environment for osteoblast-like cell proliferation. Furthermore, compared to PCL-forsterite porous scaffolds developed in our previous report (Diba et al., 2012) application of the fine fibrous structure is expected to have improved cellular interactions due to simulation of ECM structure, ability to guide the cells to grow at the specific directions, presence of the large surface area-to-volume ratio and interconnected porosity which are considered essential for cellular growth in-vitro and in-vivo as they are directly involved in the transport of oxygen and nutrients to the cells.

Additionally, the quantification data of the mineral deposition obtained by alizarin red assay (Fig. 7(c)) demonstrated the presence of mineralized bone nodules on the cell surfaces cultured on the membranes. At day 21 of culture, the measured absorbance of the eluents, which is proportional to MC-3T3 mineralization, collected from A(P-20F) membrane was significantly ($P<0.05$) higher than that of on A(PCL) and A

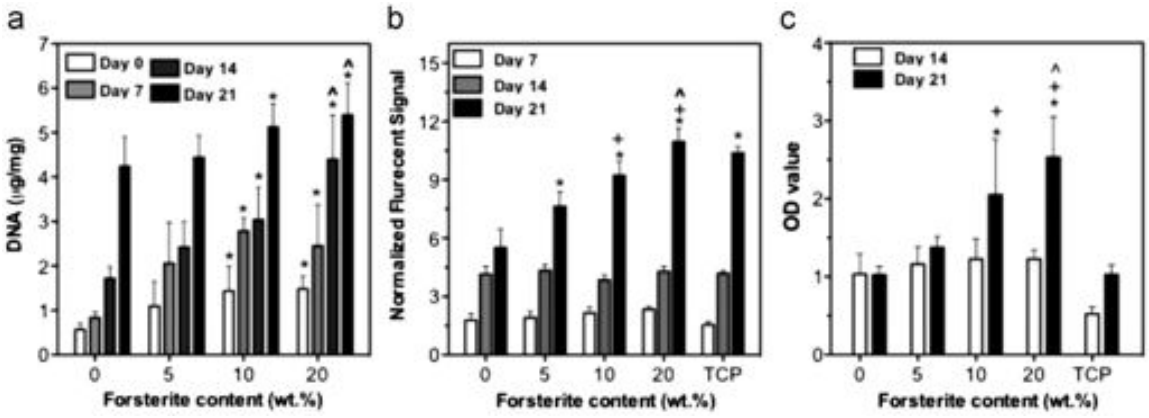

Fig. 7 – Effects of forsterite content on the interaction cellular responses: (a) DNA quantification of MC-3T3 cells cultured for 6 h, 7, 14 and 21 days on the aligned fibrous membranes. (b) Normalized MC-3T3 cell metabolic activity determined by Alamar Blue assay at days 7, 14 and 21 of culture. (c) Alizarin Red-S staining of mineral deposition on the fibrous membranes (*, ^, +: significant difference compared to A(PCL), A(P-5F) and TCP, respectively (*,^, +: $P<0.05$)).

(P-5F) membranes. The process of mineralized nodule formation has three main developmental stages: proliferation, development of ECM and mineralization (Aubin, 1998). According to above results, either significantly greater proliferation of MC-3T3 cells on A(P-10F) and A(P-20F) or about two and three-fold mineral depositions on A(P-10F) and A(P-20F), respectively, compared to that of on A(PCL) membrane confirmed the enhancement of mineralized nodule formation. Furthermore, as higher amount of mineral deposits implies a higher degree of MC-3T3 differentiation, enhanced bone formation ability can be expected from fibrous PCL-forsterite fibrous membranes.

This study was focused on the development of nanofibrous composite membranes of PCL-forsterite and assessment on their properties for potential GBR application. According to previous results, the optimal biodegradable membrane for GBR has to be strong, able to stimulate bone formation and promote pre-osteoblast proliferation and differentiation. PCL is frequently used in electrospinning processing to produce nanofibrous scaffolds and membranes for bone tissue engineering application. However, as a GBR membrane, forsterite nanopowder improved the properties of PCL such as the bioactivity, degradation and rigidity. According to these data, forsterite nanopowder enhanced the formation of new bone tissue by increasing osteoblast attachment, proliferation and deposition of calcium-containing minerals on the nanofibrous composite membranes, which might be attractive as a GBR membrane.

4. Conclusions

In the present study, novel randomly-oriented and aligned nanofibrous composite membranes of PCL and forsterite nanopowder were successfully developed through electrospinning technique. Addition of forsterite nanopowder increased the hydrophilicity, bioactivity, degradable ability and mechanical properties of pure PCL fibrous membranes. Furthermore, aligned fibrous membranes exhibited anisotropic mechanical properties, while compared to the randomly oriented nanofibrous membranes they exhibited higher tensile strength, tensile modulus and strain to failure. Results showed that aligned fibrous membranes consisting of 10 wt% forsterite nanopowder exhibited the smallest average fiber diameters and significantly increased mechanical properties. However, the membrane with 20 wt% forsterite nanopowder loading exhibited lower mechanical properties and larger fiber sizes indicated agglomeration and the heterogeneity of the structure. Forsterite nanopowder also enhanced the attachment, proliferation and mineralization of pre-osteoblast cells. We believe that PCL-forsterite nanofibrous membranes nanofibers may have potential applications as a GBR membrane.

Acknowledgments

The authors are grateful for support of this research by Isfahan University of Technology.

REFERENCES

Aubin, J.E., 1998. Advances in osteoblast lineage. Bioechemistry and Cell Biology 76, 899–910.

Bianco, A., Federico, E.D., Moscatelli, I., Camaion, A., Armentano, I., Campagnolo, L., Dottori, M., Kenny, J.M., Siracusa, G., Gusmano, G., 2009. Electrospun poly(ε-caprolactone)/Ca-deficient hydroxyapatite nanohybrids: Microstructure, mechanical properties and cell response by murine embryonic stem cells. Materials Science and Engineering C 29, 2063–2071.

Bishop, A., Balazsi, C., Yang, J.H.C., Gouma, P.I., 2006. Biopolymer–hydroxyapatite by electrospinning. Polymers for Advanced Technologies 17, 902–906.

Catledge, S.A., Clem, W.C., Shrikishen, N., Chowdhury, S., Stanishevsky, A.V., Koopman, M., 2007. An electrospun triphasic nanofibrous scaffold for bone tissue engineering. Biomedical Materials 2, 142–150.

Deng, X.L., Sui, G., Zhao, M.L., Chen, G.Q., Yang, X.P., 2007. Poly(L-lactic acid)/hydroxyapatite hybrid nanofibrous scaffolds prepared by electrospinning. Journal of Biomaterials Science, Polymer Edition 18, 117–130.

Denry, I.L., 1996. Recent advances in ceramics for dentistry. Critical Reviews in Oral Biology and Medicine 7 (2), 134–143.

Diba, M., Fathi, M.H., Kharaziha, M., 2011. Novel forsterite/ polycaprolactone nanocomposite scaffold for tissue engineering applications,. Materials Letters 65, 1931–1934.

Diba, M., Kharaziha, M., Fathi, M.H., Gholipourmalekabadi, M., Samadikuchaksaraei, A., 2012. Preparation and characterization of polycaprolactone/forsterite nanocomposite porous scaffolds designed for bone tissue regeneration. Composites Science and Technology 72, 716–723.

Du, C., Cui, F.Z., Zhu, X.D., De Groot, K., 1999. Three-dimensional nano-HAp/ collagen matrix loading with osteogenic cells in organ culture. Journal of Biomedical Materials Research 44, 407–415.

Fu, S., Ni, P., Wang, B., Chu, B., Peng, J., Zheng, L., Zhao, X., Luo, F., Wei, F., Qian, Z., 2012. In vivo biocompatibility and osteogenesis of electrospun poly(ε-caprolactone)epoly (ethylene glycol),poly(ε-caprolactone)/ nano-hydroxyapatite composite scaffold. Biomaterials 33, 8363–8371.

Fujihara, K., Kotaki, M., Ramakrishna, S., 2005. Guided bone regeneration membrane made of polycaprolactone/ calcium carbonate composite nano-fibers. Biomaterials 26, 4139–4147.

Jose, M.V., Thomas, V., Johnson, K.T., Dean, D.R., Nyairo, E., 2009. Aligned PLGA/HA nanofibrous nanocomposite scaffolds for bone tissue engineering. Acta Biomaterialia 5, 305–315.

Kharaziha, M., Fathi, M.H., 2009. Synthesis and characterization of bioactive forsterite nanopowder. Ceramics International 35, 2449–2454.

Kharaziha, M., Fathi, M.H., 2010. Improvement of mechanical properties and biocompatibility of forsterite bioceramic addressed to bone tissue engineering materials. Journal of the Mechanical Behavior of Biomedical Materials 1, 530–537.

Kim, H.W., Song, J.H., Kim, H.E., 2005. Nanofiber generation of gelatin-hydroxyapatite biomimetics for guided tissue regeneration. Advanced Functional Materials 15, 1988–1994.

Kokubo, T., Takadama, H., 2006. How useful is SBF in predicting in vivo bone bioactivity?. Biomaterials 27, 2907–2915.

Lee, E.J., Teng, S.H., Jang, T.S., Wang, P., Yook, S.W., Kim, H.E., Koh, E.H., 2010. Nanostructured poly(e-caprolactone)–silica xerogel fibrous membrane for guided bone regeneration. Acta Biomaterialia 6, 3557–3565.

Lehmann, G., Palmero, P., Cacciotti, I., Pecci, R., Campagnolo, L., Bedini, R., et al., 2010. Design, production and biocompatibility of nanostructured and porous HAp and Si-HAp ceramics as three-dimensional scaffolds for stem cell culture and differentiation. Ceramics-Silikáty 54, 90–96.

Liang, D., Hsiao, B.S., Chu, B., 2007. Functional electrospun nanofibrous scaffolds for biomedical applications. Advanced Drug Delivery Reviews 59, 1392–1412.

Low, V.S., Choon, A.T., Kumar, A.B., Ramakrishna, S., 2008. Electrospun-modified nanofibrous scaffolds for the mineralization of osteoblast cells. Journal of Biomedical Materials Research 85, 408.

Ni, S., Cho, U.L., Chang, J., 2007. Preparation and characterization of forsterite (Mg_2SiO_4) bioceramics. Ceramics International 33, 83–88.

Obata, A., Hotta, T., Wakita, T., Ota, Y., Kasuga, T., 2010. Electrospun microfiber meshes of silicon-doped vaterite/poly (lactic acid) hybrid for guided bone regeneration. Acta Biomaterialia 6, 1248–1257.

Park, S.H., Wang, H.L., 2007. Clinical significance of incision location on guided bone regeneration: human study. Journal of Periodontolology 78, 47–51.

Poologasundarampillai, G., Fujikura, K., Obata, A., Kasuga, T., 2011. Modification and mechanical properties of electrospun blended fibermat of PLGA and siloxane-containing vaterite/ PLLA hybrids for bone repair. Polymer Letters 5 (10), 873–881.

Sui, G., Yang, X., Mei, F., Hu, X., Chen, G., Deng, X., Ryu, S., 2007. Poly-L-lactic acid/hydroxyapatite hybrid membrane for bone tissue regeneration. Journal of Biomedical Materials Research A 82 (2), 445–454.

Thomas, V., Jagani, S., Johnson, K., Jose, M.V., Dean, D.R., Vohra, Y.K., et al., 2006. Electrospun bioactive nanocomposite scaffolds of polycaprolactone and nano-hydroxyapatite for bone tissue engineering. Journal for Nanoscience and Nanotechnology 6, 487–493.

Thomas, V., Dean, D.R., Jose, M.V., Mathew, B., Chowdhury, S., Vohra, Y.K., 2007. Nanostructured biocomposite scaffolds based on collagen co-electrospun with nanohydroxyapatite. Biomacromolecules 8, 631–637.

Tyagi, P., Catledge, S.A., Stanishevsky, A., Thomas, V., Vohra, Y.K., 2009. Nanomechanical properties of electrospun composite scaffolds based on polycaprolactone and hydroxyapatite. Journal for Nanoscience and Nanotechnology 9, 4839–4845.

Webster, T.J., Ergun, C., Doremus, R.H., Siegel, R.W., Bizios, R., 2000. Specific proteins mediate enhanced osteoblast adhesion on nanophase ceramics. Journal of Biomedical Materials Research 21, 475–483.

Woodruff, A., Hutmacher, D.W., 2010. The return of a forgotten polymer— polycaprolactone in the 21st century. Progress in Polymer Science 35 (10), 1217–1256.

Xu, C.Y., Inai, R., Kotaki, M., Ramakrishna, S., 2004. Aligned biodegradable nanofibrous structure: a potential scaffold for blood vessel engineering. Biomaterials 25, 877–886.

Yang, F., Both, S.K., Yang, X., Walboomers, X.F., Jansen, J.A., 2009. Development of an electrospun nano-apatite/PCL composite membrane for GTR/GBR application. Acta Biomaterialia 5, 3295–3304.

Yang, K.K., Wang, X.L., Wang., Y.Z., 2007. Progress in Nanocomposite of Biodegradable Polymer. Journal of Industrial and Engineering Chemistry 13, 485.